Loss-of-function mutation in Omicron variants reduces spike protein expression and attenuates SARS-CoV-2 infection

Michelle N. Vu[1], R. Elias Alvarado[1,2], Dorothea R. Morris[1,3], Kumari G. Lokugamage[1], Yiyang Zhou[4], Angelica L. Morgan[5], Leah K. Estes[1], Alyssa M. McLeland[1], Craig Schindewolf[1], Jessica A. Plante[1,6,7], Yani P. Ahearn[1], William M. Meyers[5], Jordan T. Murray[1], Patricia A. Crocquet-Valdes[5], Scott C. Weaver[1,6,7,8], David H. Walker[5,8], William K. Russell[4], Andrew L. Routh[4], Kenneth S. Plante[1,6,7], Vineet Menachery[1,6,7,8*]

[1]Microbiology and Immunology, University of Texas Medical Branch, Galveston, TX, United States.
[2]Institute for Translational Sciences, University of Texas Medical Branch, Galveston, TX, United States.
[3]Pediatrics, University of Texas Medical Branch, Galveston, TX, United States.
[4]Biochemistry and Molecular Biology, University of Texas Medical Branch, Galveston, TX, United States.
[5]Pathology, University of Texas Medical Branch, Galveston, TX, United States.
[6]Institute for Human Infection and Immunity, University of Texas Medical Branch, Galveston, TX, United States.
[7]World Reference Center of Emerging Viruses and Arboviruses, University of Texas Medical Branch, Galveston, TX, United States.
[8]Center for Biodefense and Emerging Infectious Disease, University of Texas Medical Branch, Galveston, TX, United States.

* Corresponding Author: Vineet D. Menachery, vimenach@utmb.edu

Abstract

SARS-CoV-2 Omicron variants emerged in 2022 with >30 novel amino acid mutations in the spike protein alone. While most studies focus on receptor binding domain changes, mutations in the C-terminus of S1 (CTS1), adjacent to the furin cleavage site, have largely been ignored. In this study, we examined three Omicron mutations in CTS1: H655Y, N679K, and P681H. Generating a SARS-CoV-2 triple mutant (YKH), we found that the mutant increased spike processing, consistent with prior reports for H655Y and P681H individually. Next, we generated a single N679K mutant, finding reduced viral replication *in vitro* and less disease *in vivo.* Mechanistically, the N679K mutant had reduced spike protein in purified virions compared to wild-type; spike protein decreases were further exacerbated in infected cell lysates. Importantly, exogenous spike expression also revealed that N679K reduced overall spike protein yield independent of infection. Although a loss-of-function mutation, transmission competition demonstrated that N679K had a replication advantage in the upper airway over wild-type SARS-CoV-2 in hamsters, potentially impacting transmissibility. Together, the data show that N679K reduces overall spike protein levels during Omicron infection, which has important implications for infection, immunity, and transmission.

40 **Introduction**

41 Since its introduction, SARS-CoV-2 has continuously evolved giving rise to multiple
42 Variants of Concern (VOCs) with diverse mutations in the spike protein [1] (**Extended Fig. 1A**).
43 Present as a trimer on virions, spike is composed of S1 and S2 subunits, responsible for receptor
44 binding and membrane fusion, respectively [2,3]. The S1 subunit contains the N-terminal domain
45 (NTD), receptor binding domain (RBD), and the C-terminus of the S1 subunit (CTS1), which
46 harbors a furin cleavage site (FCS) in SARS-CoV-2. Following receptor binding, the spike is
47 cleaved at the S1/S2 site by host proteases to expose the fusion machinery for entry. With the
48 diverse mutations in the spike protein (**Extended Fig. 1B**), most Omicron studies have focused
49 on the RBD and the impact on vaccine- or infection-induced immunity. However, mutations
50 surrounding the FCS and S1/S2 cleavage site have been demonstrated to drive SARS-CoV-2
51 pathogenesis [4-9] and have been largely unstudied in the context of Omicron.

52 With this in mind, we set out to evaluate the role of Omicron CTS1 mutations on infection
53 and pathogenesis. Omicron maintains three mutations adjacent to the FCS and S1/S2 cleavage
54 site: H655Y, N679K, and P681H (**Extended Fig. 1B**). Both H655Y and P681H have previously
55 been observed in the Gamma and Alpha variants [10,11]; in contrast, N679K is unique to and
56 maintained by all Omicron subvariants [12]. To evaluate the role of these mutations, we used
57 reverse genetics to generate SARS-CoV-2 mutants with all three CTS1 mutations (YKH) or
58 N679K alone in the original WA1 backbone from early 2020. While YKH modestly increases viral
59 replication and spike processing *in vitro*, N679K results in a loss-of-function mutation that
60 attenuates viral replication *in vitro* and disease *in vivo* while skewing replication toward the upper
61 airways through reduced spike protein expression. Given the importance of spike protein for
62 immunity, our finding may have major implications for vaccine efficacy and breakthrough
63 infections.

64

Results

H655Y, N679K, and P681H together increase viral replication and spike processing.

While the majority of the > 30 spike mutations Omicron acquired are localized to the RBD, three are harbored in the CTS1 adjacent to the furin cleavage site – H655Y, N679K, and P681H (**Fig. 1A**). Both H655Y and P681H have been observed individually in Gamma and Alpha variants and are associated with increased spike processing. In contrast, N679K is a mutation unique to Omicron and is maintained in all subsequent Omicron subvariants despite involving a single nucleotide change (T/C to A/G) in the wobble codon position [12]. Importantly, N679K is adjacent to an important O-linked glycosylation site at T678 [13,14]; our group has previously shown this glycosylation is important for SARS-CoV-2 infection and protease usage [8].

Several motifs within the CTS1 spike domain, including the furin cleavage site and the upstream QTQTN motif, are key to spike cleavage and host protease interactions, which drive SARS-CoV-2 infection and pathogenesis. All three Omicron mutations in the CTS1, H655Y, N679K, and P681H, are adjacent to or within these motifs and may impact their function (**Fig. 1A and 1B**). To evaluate this, we generated a mutant SARS-CoV-2 harboring H655Y, N679K, and P681H in the original WA1 backbone (YKH) (**Fig. 1C**) [15,16]. Plaques produced by the YKH mutant were smaller compared to the parental WA1 (WT) (**Fig. 1D**). However, the YKH mutant did not attenuate stock titers nor replication kinetics in Vero E6 cells as compared to wild-type (WT) SARS-CoV-2 (**Fig. 1E and 1F**). Notably, while replication was slightly reduced at 24 hpi, end point titers for YKH were augmented at 48 hpi in Calu-3 2B4 cells compared to WT (**Fig. 1G**). The results suggest that the combination of the three mutations alters infection dynamics, which may offer some advantages to the Omicron variant in human respiratory cells (**Fig. 1G**). As H655Y and P681H have individually been shown to increase spike processing, we next evaluated spike processing on purified virions from YKH and WT infection. Similar to Delta and Omicron, YKH spike was more processed than WT (**Fig. 1H and 1I**). At 24 hpi, the S1/S2 cleavage ratio to full length spike ratio was ~2.4:1 for the YKH spike (55% S1/S2 product, 23% full-length); in contrast,

91 WT had roughly equivalent amounts of S1/S2 product and full length. Overall, the combination of
92 H655Y, N679K, and P681H in the YKH mutant resulted in increased viral endpoint yields in human
93 respiratory cells and contributed to Omicron's enhanced spike processing.

94 **N679K mutation attenuates SARS-CoV-2 infection.**

95 The increase in spike processing found in the YKH mutant is consistent with prior work
96 examining H655Y and P681H mutations individually; however, the contribution of N679K had yet
97 to be evaluated. Based on its location adjacent to a key O-linked glycosylation site [8], we
98 hypothesized that N679K might impact SARS-CoV-2 infection (**Fig. 2A**). To evaluate potential
99 changes, we generated a SARS-CoV-2 mutant with only N679K in the WA1 backbone (N679K)
100 (**Fig. 2B**). Our initial characterization found that the N679K plaque sizes were distinctly smaller at
101 days 2 and 3 post-infection (**Fig. 2C**), and stock titers were also slightly lower than WT (**Fig. 2D**).
102 These differences in plaque size and stock titers are consistent with observations of most Omicron
103 strains [17-20]. Notably, unlike the minimal differences seen in YKH replication kinetics, the N679K
104 mutant had attenuated replication in both Vero E6 and Calu-3 2B4 cells at 24 hpi (**Fig. 2E and**
105 **2F**). Although N679K viral titer recovered by 48 hpi, the results suggest that N679K is a loss-of-
106 function mutation in terms of replication in both cell lines.

107 We next evaluated N679K *in vivo* by infecting 3-to-4-week-old golden Syrian hamsters
108 and monitored weight loss and disease over 7 days (**Fig. 2G**). Hamsters infected with N679K
109 displayed significantly attenuated body weight loss compared to those infected with WT (**Fig. 2H**).
110 Despite the stark attenuation seen in weight loss, N679K viral titers in the lungs were equivalent
111 to WT at 2 dpi and 4 dpi (**Fig. 2I**). Similarly, N679K viral titers were comparable to WT at 2 dpi in
112 nasal washes; however, the mutant virus resulted in reduced replication at 4 dpi (**Fig. 2J**). In
113 addition, analysis of lung histopathology showed a modest, but not significant reduction in disease
114 of the N679K infected hamsters as compared to control (**Extended Fig. 2**). Taken together, our
115 results indicate that N679K has a distinct loss-of-function phenotype *in vitro* and *in vivo*.

116 **N679K mutation results in decreased spike protein expression.**

117 We next sought to determine the mechanism driving the loss-of-function observed with
118 the N679K mutant. Given its location adjacent to the FCS, we first evaluated N679K effects on
119 proteolytic spike processing. Virions were purified from WT, N679K or the Omicron variant BA.1
120 (Omicron) and blotted for spike processing. Nearly identical to YKH, the N679K mutant had
121 increased spike processing with a ~2.5:1 ratio of S1/S2 cleavage product to full-length spike
122 compared to 1:1 ratio for WT at 24 hpi (**Fig. 3A and 3B**). However, we noted distinct differences
123 in total spike protein with N679K and Omicron compared to WT, despite similar levels of
124 nucleocapsid protein. Densitometry analysis revealed that the total spike to nucleocapsid (S/N)
125 ratio of N679K and Omicron virions was reduced 21% and 36%, respectively, as compared to WT
126 (**Fig. 3C**). Overall, our results indicate that the N679K mutant and Omicron variant incorporate
127 less spike protein into their virions.

128 We then sought to determine if changes in the virion spike were due to changes to total
129 protein expression in the cell or spike incorporation into the particle. To examine spike protein
130 expression, we measured total spike relative to nucleocapsid from infected Vero E6 cell lysates
131 24 hpi (**Fig. 3D and 3E**). N679K resulted in a S/N ratio 66% less than WT, displaying an even
132 further decrease in spike protein compared to the reduction in purified virions. Additionally, a
133 similar decrease in S/N ratio was observed in Omicron, indicating that the phenotype is
134 maintained in the context of all the Omicron mutations (**Fig. 3D and 3E**). Importantly, the RNA
135 transcript ratio for both spike and N following infection of WT and N679K were nearly identical
136 indicating no deficits in RNA expression of spike in the mutant (**Fig. 3F**). Together, the results
137 indicate that the N679K mutation reduces the Omicron spike protein levels compared to WT
138 following infection.

139 Having established reduced spike protein in the context of N679K, we next wanted to
140 determine if this reduction only occurs in the context of virus infection or is inherent to the protein.
141 Therefore, we introduced the mutation into the Spike HexaPro plasmid to exogenously express
142 spike protein and separate N679K driven changes from other aspects of viral infection [21]. Vero

143 E6 cells were transfected with the WT or N679K mutant spike HexaPro and harvested at 24 and
144 48 hours post transfection (hpt). Similar to what was observed in viral infection, N679K spike was
145 reduced 43% at 24 hpt and 46% at 48 hpt (**Fig. 3G and 3H**). Overall, the results across virions,
146 cell lysates, and overexpression systems demonstrate that the reduction in spike protein is
147 governed by the N679K mutation in a manner independent of viral infection (**Fig. 3I**).

148 **N679K mutation results in preference for the upper airways.**

149 Recognizing that decreased spike expression impacts virus infection, we next evaluated
150 the role of N679K on SARS-CoV-2 transmissibility. Using transmission competition, donor
151 hamsters were infected with a 1:1 ratio of WT:N679K SARS-CoV-2 at a total of 10^5 pfu **(Fig. 4A)**.
152 At 24 hpi, donors were paired with naïve recipients, cohoused for 8 hrs, separated, and donors
153 nasal washed. Nasal wash, trachea, and lung were collected to measure viral RNA populations
154 at 2 and 4 days post infection (dpi) for donors and post contact (dpc) for recipients. Surprisingly,
155 while both viruses transmitted, WT and N679K demonstrated distinct replication sites along the
156 respiratory tract **(Fig. 4B)**. N679K dominated the nasal washes and upper airways while WT
157 primarily seeded the lungs and lower airways. The trachea serves as a midpoint, with no clear
158 delineation between the viruses **(Fig. 4B)**. Having observed this gradation, we returned to the
159 prior hamster study and examined antigen staining of the lung **(Fig. 4C)**. While no significant
160 differences in total antigen were noted, the localization of viral antigen in the N679K infection was
161 distinct and concentrated in the large airways. In contrast, WT was more uniformly distributed in
162 the parenchyma and airways **(Fig. 4D)**. Overall, the results indicate that the N679K mutation shifts
163 viral replication towards airway replication.

164 **Discussion**

165 Most Omicron studies have focused on determining the impact that the RBD mutations
166 have on immune escape, largely overlooking mutations in other spike domains like the CTS1.
167 Harboring the FCS and S1/S2 cleavage site, the CTS1 has been demonstrated as a hotspot for
168 both attenuating and augmenting mutations [4-9]. Focusing on Omicron's three CTS1 mutations –

169 H655Y, N679K, and P681H, we generated infectious clones with all three (YKH) or N679K alone
170 in the SARS-CoV-2 WA1 background. The combination of YKH produced a modest increase in
171 endpoint titers after infection of human respiratory cells, and augmented spike processing,
172 consistent with prior studies that tested the effects of H655Y and P681H individually [10,11].
173 However, the N679K mutant reduced viral replication *in vitro* and weight loss *in vivo*. Mechanistic
174 studies determined that both N679K and Omicron have reduced spike protein incorporated into
175 their virions, less spike protein in infected cell lysates, and inferior production using exogenous
176 spike protein expression systems. Our results argue that reduced spike protein in the context the
177 N679K mutation attenuates Omicron strains and may have implications for SARS-CoV-2
178 immunity by reducing spike antigen thus shifting immune recognition. Additionally, while the
179 N679K mutation attenuated the virus *in vivo*, our studies indicate a shift toward the upper airways
180 replication. Overall, the data argue that N679K acts as a loss-of-function mutation that has a
181 significant impact on SARS-CoV-2 Omicron infection, pathogenesis, and transmission dynamics.
182 N679K is likely attenuated because of its decrease in spike protein production. Starting
183 with ~20-30% less spike in its virions, one possibility was a change in spike incorporation.
184 However, an even greater decrease (66%) in spike protein was present in infected Vero E6 cell
185 lysates, indicated that overall spike protein levels were affected. In addition, we found no change
186 in the ratio of spike message relative to N transcript, suggesting the N679K mutation impacts the
187 protein itself. To confirm that the reduction in spike was not a product of virus infection or host
188 immune interactions, we exogenously expressed the spike protein to demonstrate that the N679K
189 spike protein itself was less stable than the WT control. One possible mechanism is that the
190 asparagine-to-lysine change introduces a ubiquitination site that could lead to spike degradation.
191 Another possible mechanism is that the N679K mutation itself may destabilize the protein
192 structurally. Additionally, the N679K substitution adds another basic amino acid to the stretch
193 including the furin cleavage site; the positively charged lysine extends the polybasic cleavage
194 motif and may facilitate cleavage by additional host proteases [22]. Overall, while the exact

195 mechanism is unclear, the N679K mutation results in a less stable spike protein that impacts
196 infection and pathogenesis of SARS-CoV-2.

197 Surprisingly, N679K is uniformly found in 100% of Omicron sequences in GSAID, despite
198 being a single nucleotide change in the wobble position [12]. Though attenuated *in vitro*, N679K
199 does replicate to similar titers as WT in hamster lungs and at day 2 in nasal washes. Notably,
200 N679K outcompetes WT in the upper airways when in direct transmission competition. These
201 results suggest no deficits in transmission and may augment spread as virus replication in the
202 upper airway is more likely to seed new infections. These results also potentially explain why
203 N679K is maintained despite clear attenuation of SARS-CoV-2 infection. Notably, addition of
204 H655Y and P681H in the YKH mutant rescues replication in Calu-3 cells, suggesting that other
205 Omicron mutations may compensate for N679K. However, it is unclear if reverting N679K in the
206 Omicron strains would result in a gain in terms of *in vitro* replication or *in vivo* pathogenesis. While
207 N679K in SARS-CoV-2 WA1 produces a clear loss-of-function, the constellation of spike
208 mutations and epistatic interactions may mitigate the deficit in Omicron strains. Importantly, the
209 complete conservation of N679K in Omicron also implies some fitness advantage [23-28]. From our
210 data, the shift toward upper airway replication by N679K may explain how it is maintained despite
211 lower overall spike protein expression.

212 In addition to impacting primary infection, the reduction in spike protein may have
213 important implications for SARS-CoV-2 and human immunity. Compared to WT, the N679K
214 mutant produces less spike protein upon infection and can potentially skew the ratio of antibodies
215 targeting spike and nucleocapsid. Prior work with SARS-CoV had shown that an altered
216 spike/nucleocapsid antibody ratio contributed to vaccine failure in aged mice [29]. Therefore,
217 infection with Omicron could increase N targeting antibodies at the expense of spike antibodies.
218 The result would be less protective neutralizing antibody, which may facilitate more breakthrough
219 infections. Furthermore, SARS-CoV-2 vaccines based on the Omicron spike may produce less
220 spike protein due to N679K mutation. In the context of the mRNA bivalent vaccines, the N679K

221 mutation may alter the 1:1 ratio of WT to Omicron spike protein; N679K may bias immune
222 responses towards WT spike protein instead of equally between both spike proteins. In addition,
223 the total amount of spike protein produced may be less than previous vaccines formulations, thus
224 diminishing the overall antibody response. These factors potentially contribute to the less than
225 expected increase in immunity against Omicron strains despite the new bivalent vaccine
226 formulations. Moving forward, reverting K679 back to N679 in vaccine may improve spike protein
227 yields and subsequently improve vaccine response to the Omicron variants.

228 Together, our results demonstrate that Omicron N679K is a loss-of-function mutation
229 consistently maintained in subvariants. Mechanistically, the N679K mutation attenuates the virus
230 *in vitro* and *in vivo* by increasing spike degradation. While the N679K mutation is attenuating in
231 isolation, other Omicron mutations like H655Y and P681H may compensate for the N679K loss
232 of function by amplifying spike processing and infection. However, the decreased spike protein
233 expression by N679K may have implications for immunity induced by infection and vaccines. In
234 addition, while N679K attenuated viral pathogenesis, the shift to the upper airway replication may
235 have enhanced transmissibility and contribute to Omicron emergence. Overall, the data highlight
236 that the Omicron CTS1 mutations have a significant impact on SARS-CoV-2 infection and are
237 worthy of continued study and surveillance.

References

1 Callaway, E. Heavily mutated Omicron variant puts scientists on alert. *Nature* **600**, 21 (2021). https://doi.org:10.1038/d41586-021-03552-w

2 Belouzard, S., Millet, J. K., Licitra, B. N. & Whittaker, G. R. Mechanisms of Coronavirus Cell Entry Mediated by the Viral Spike Protein. *Viruses* **4**, 1011-1033 (2012).

3 Vu, M. N. & Menachery, V. D. Binding and entering: COVID finds a new home. *PLOS Pathogens* **17**, e1009857 (2021). https://doi.org:10.1371/journal.ppat.1009857

4 Coutard, B. *et al.* The spike glycoprotein of the new coronavirus 2019-nCoV contains a furin-like cleavage site absent in CoV of the same clade. *Antiviral Research* **176**, 104742 (2020). https://doi.org:https://doi.org/10.1016/j.antiviral.2020.104742

5 Johnson, B. A. *et al.* Loss of furin cleavage site attenuates SARS-CoV-2 pathogenesis. *Nature* (2021). https://doi.org:10.1038/s41586-021-03237-4

6 Liu, Y. *et al.* Delta spike P681R mutation enhances SARS-CoV-2 fitness over Alpha variant. *bioRxiv*, 2021.2008.2012.456173 (2021). https://doi.org:10.1101/2021.08.12.456173

7 Peacock, T. P. *et al.* The furin cleavage site in the SARS-CoV-2 spike protein is required for transmission in ferrets. *Nat Microbiol* **6**, 899-909 (2021). https://doi.org:10.1038/s41564-021-00908-w

8 Vu, M. N. *et al.* QTQTN motif upstream of the furin-cleavage site plays a key role in SARS-CoV-2 infection and pathogenesis. *Proceedings of the National Academy of Sciences* **119**, e2205690119 (2022). https://doi.org:doi:10.1073/pnas.2205690119

9 Lau, S.-Y. *et al.* Attenuated SARS-CoV-2 variants with deletions at the S1/S2 junction. *Emerging Microbes & Infections* **9**, 837-842 (2020). https://doi.org:10.1080/22221751.2020.1756700

10 Escalera, A. *et al.* Mutations in SARS-CoV-2 variants of concern link to increased spike cleavage and virus transmission. *Cell Host & Microbe* **30**, 373-387.e377 (2022). https://doi.org:10.1016/j.chom.2022.01.006

11 Liu, Y. *et al.* Delta spike P681R mutation enhances SARS-CoV-2 fitness over Alpha variant. *Cell Reports* **39** (2022). https://doi.org:10.1016/j.celrep.2022.110829

12 Hadfield, J. *et al.* Nextstrain: real-time tracking of pathogen evolution. *Bioinformatics* **34**, 4121-4123 (2018). https://doi.org:10.1093/bioinformatics/bty407

13 Gao, C. *et al.* SARS-CoV-2 Spike Protein Interacts with Multiple Innate Immune Receptors. *bioRxiv*, 2020.2007.2029.227462 (2020). https://doi.org:10.1101/2020.07.29.227462

14 Sanda, M., Morrison, L. & Goldman, R. N- and O-Glycosylation of the SARS-CoV-2 Spike Protein. *Anal Chem* **93**, 2003-2009 (2021). https://doi.org:10.1021/acs.analchem.0c03173

15 Xie, X. *et al.* An Infectious cDNA Clone of SARS-CoV-2. *Cell Host Microbe* **27**, 841-848 e843 (2020). https://doi.org:10.1016/j.chom.2020.04.004

16 Xie, X. *et al.* Engineering SARS-CoV-2 using a reverse genetic system. *Nature Protocols* **16**, 1761-1784 (2021). https://doi.org:10.1038/s41596-021-00491-8

17 Peacock, T. P. *et al.* The altered entry pathway and antigenic distance of the SARS-CoV-2 Omicron variant map to separate domains of spike protein. *bioRxiv*, 2021.2012.2031.474653 (2022). https://doi.org:10.1101/2021.12.31.474653

18 Meng, B. *et al.* Altered TMPRSS2 usage by SARS-CoV-2 Omicron impacts infectivity and fusogenicity. *Nature* **603**, 706-714 (2022). https://doi.org:10.1038/s41586-022-04474-x

19 Phadke, K. S., Higdon, N. B. A. & Bellaire, B. H. In vitro comparison of SARS-CoV-2 variants. *bioRxiv*, 2023.2003.2011.532212 (2023). https://doi.org:10.1101/2023.03.11.532212

20 Zhao, H. *et al.* SARS-CoV-2 Omicron variant shows less efficient replication and fusion activity when compared with Delta variant in TMPRSS2-expressed cells. *Emerging Microbes & Infections* **11**, 277-283 (2022). https://doi.org:10.1080/22221751.2021.2023329

21 Hsieh, C.-L. *et al.* Structure-based design of prefusion-stabilized SARS-CoV-2 spikes. *Science* **369**, 1501-1505 (2020). https://doi.org:doi:10.1126/science.abd0826

22 Mustafa, Z., Kalbacher, H. & Burster, T. Occurrence of a novel cleavage site for cathepsin G adjacent to the polybasic sequence within the proteolytically sensitive activation loop of the SARS-CoV-2 Omicron variant: The amino acid substitution N679K and P681H of the spike protein. *PLOS ONE* **17**, e0264723 (2022). https://doi.org:10.1371/journal.pone.0264723

23 Yuan, S. *et al.* Pathogenicity, transmissibility, and fitness of SARS-CoV-2 Omicron in Syrian hamsters. *Science* **377**, 428-433 (2022). https://doi.org:doi:10.1126/science.abn8939

24 McCormack, C. P. *et al.* Modelling the viral dynamics of the SARS-CoV-2 Delta and Omicron variants in different cell types. *bioRxiv*, 2023.2003.2015.529513 (2023). https://doi.org:10.1101/2023.03.15.529513

25 Hui, K. P. Y. *et al.* SARS-CoV-2 Omicron variant replication in human bronchus and lung ex vivo. *Nature* **603**, 715-720 (2022). https://doi.org:10.1038/s41586-022-04479-6

26 Carabelli, A. M. *et al.* SARS-CoV-2 variant biology: immune escape, transmission and fitness. *Nature Reviews Microbiology* **21**, 162-177 (2023). https://doi.org:10.1038/s41579-022-00841-7

27 Papanikolaou, V. *et al.* From delta to Omicron: S1-RBD/S2 mutation/deletion equilibrium in SARS-CoV-2 defined variants. *Gene* **814**, 146134 (2022). https://doi.org:https://doi.org/10.1016/j.gene.2021.146134

28 Shrestha, L. B., Foster, C., Rawlinson, W., Tedla, N. & Bull, R. A. Evolution of the SARS-CoV-2 omicron variants BA.1 to BA.5: Implications for immune escape and transmission. *Reviews in Medical Virology* **32**, e2381 (2022). https://doi.org:https://doi.org/10.1002/rmv.2381

29 Deming, D. *et al.* Vaccine Efficacy in Senescent Mice Challenged with Recombinant SARS-CoV Bearing Epidemic and Zoonotic Spike Variants. *PLOS Medicine* **3**, e525 (2006). https://doi.org:10.1371/journal.pmed.0030525

30 Harcourt, J. *et al.* Severe Acute Respiratory Syndrome Coronavirus 2 from Patient with Coronavirus Disease, United States. *Emerging infectious diseases* **26**, 1266-1273 (2020). https://doi.org:10.3201/eid2606.200516

31 Johnson, B. A. *et al.* Nucleocapsid mutations in SARS-CoV-2 augment replication and pathogenesis. *PLOS Pathogens* **18**, e1010627 (2022). https://doi.org:10.1371/journal.ppat.1010627

32 Jaworski, E. *et al.* Tiled-ClickSeq for targeted sequencing of complete coronavirus genomes with simultaneous capture of RNA recombination and minority variants. *eLife* **10**, e68479 (2021). https://doi.org:10.7554/eLife.68479

33 Langmead, B. & Salzberg, S. L. Fast gapped-read alignment with Bowtie 2. *Nature Methods* **9**, 357-359 (2012). https://doi.org:10.1038/nmeth.1923

34 Smith, T., Heger, A. & Sudbery, I. UMI-tools: modeling sequencing errors in Unique Molecular Identifiers to improve quantification accuracy. *Genome Res* **27**, 491-499 (2017). https://doi.org:10.1101/gr.209601.116

Acknowledgments

Research was supported by grants from NIAID of the NIH to (R01-AI153602 and R21-AI145400 to VDM; R24-AI120942 (WRCEVA) to SCW). ALR was supported by a UTMB Institute for Human Infection and Immunity grant and the Sealy and Smith Foundation. Research was also supported by STARs Award provided by the University of Texas System to VDM and Data Acquisition award provided by the Institute for Human Infections and Immunity at UTMB to MNV. Trainee funding provided by NIAID of the NIH to MNV (T32-AI060549).

Mass spectrometry experiments and analysis was provided by the Mass Spectrometry Facility at the University of Texas Medical Branch (https://www.utmb.edu/MSF). Figures were created with BioRender.com

Competing Interest Statement

VDM has filed a patent on the reverse genetic system and reporter SARS-CoV-2. MNV and VDM have filed a provisional patent on a stabilized SARS-CoV-2 spike protein. Other authors declare no competing interests.

Author contributions

Conceptualization: MNV, VDM

Formal analysis: MNV, VDM

Funding acquisition: MNV, ALR, SCW, VDM

Investigation: MNV, REA, DRM, KL, CS, JAP, ALM, LKE, AMM, YPA, WMM, PAVC, JM, DHW, KP, ALR

Methodology: MNV, KSP, VDM

Project Administration: MNV, VDM

347 Supervision: MNV, SCW, DHW, KSP, VDM

348 Visualization: MNV, DHW, VDM

349 Writing – original draft: MNV, VDM

350 Writing – review and editing: MNV, REA, CS, DHW, VDM, SCW

351 **Figure Legends**

352 **Figure 1. The combination of Omicron mutations H655Y, N679K, and P681H increases viral**
353 **replication and spike processing.**

354 **(A)** Comparison of CTS1 region near the S1/S2 cleavage site between SARS-CoV-2 variants.

355 **(B)** Structure of loop containing the S1/S2 cleavage site on SARS-CoV-2 spike protein. The
356 residues that are mutated in Omicron are shown: H655 (magenta), N679 (green), and P681
357 (blue). The furin cleavage site RRAR (cyan) and QTQT motif (red) are also shown.

358 **(C)** Schematic of WT and YKH SARS-CoV-2 mutant genomes.

359 **(D)** WT and YKH SARS-CoV-2 plaques on Vero E6 cells at 2 dpi.

360 **(E)** Viral titer from WT and YKH virus stocks representing the highest yield generated from
361 TMPRSS2-expressing Vero E6 cells.

362 **(F-G)** Replication kinetics of WT and YKH in Vero E6 **(F)** and Calu-3 2B4 **(G)** cells. Cells were
363 infected at an MOI of 0.01 infectious units/cell (n=3). Data are mean ± s.d. Statistical analysis
364 measured by two-tailed Student's t-test.

365 **(H)** Purified WT, YKH, Delta isolate (B.1.617.2), and Omicron (BA.1) virions from Vero E6
366 supernatant were probed with α-Spike and α-Nucleocapsid (N) antibodies in Western blots. Full-
367 length spike (FL), S1/S2 cleavage product, and S2' cleavage product are indicated.

368 **(I)** Densitometry of FL and S1/S2 cleavage product was performed, and quantification of FL and
369 S1/S2 cleavage product percentage of total spike is shown. Quantification was normalized to N
370 for viral protein loading control. WT (black), YKH (blue), Delta isolate (purple), Omicron (orange).
371 Results are representative of two experiments.

372 **Figure 2. N679K attenuates SARS-CoV-2 replication and disease.**

373 **(A)** Structural modeling of O-linked glycosylation of threonine 678 (yellow) of QTQTN motif (red)
374 and the residues mutated in Omicron – H655 (magenta), N679 (green), and P681 (blue) – with
375 N679 adjacent to the glycosylation. The furin cleavage site RRAR is also shown (cyan).

376 **(B)** Schematic of WT and N679K SARS-CoV-2 genomes.

377 **(C)** WT and N679K SARS-CoV-2 plaques on Vero E6 cells at 2 (left) and 3 dpi (right). Average
378 plaque sizes noted below.

379 **(D)** Viral titer from WT and N679K virus stocks with the highest yield generated form TMPRSS2-
380 expressing Vero E6 cells.

381 **(E-F)** Replication kinetics of WT and N679K in Vero E6 **(E)** and Calu-3 2B4 **(F)** cells. Cells were
382 infected at an MOI of 0.01 infectious units/cell (n=3). Data are mean ± s.d. Statistical analysis
383 performed using two-tailed Student's t-test.

384 **(G)** Schematic of experimental design for golden Syrian hamster infection with WT (black) or
385 N679K (green) SARS-CoV-2. Three- to four-week-old male hamsters were infected with 10^5 pfu
386 and monitored for weight loss over 7 days. At 2, 4, and 7 dpi, nasal washes and lungs were
387 collected for viral titer, and lung was collected for histopathology.

388 **(H)** Weight loss of hamsters infected with WT (black) or N679K (green) SARS-CoV-2 over 7 days.
389 Data are mean ± s.e.m. Statistical analysis measured by two-tailed Student's t-test.

390 **(I-J)** Viral titers of lungs **(I)** and nasal washes **(J)** collected at 2 and 4 dpi from hamsters infected
391 with WT (black) or N679K (green) SARS-CoV-2. Data are mean ± s.d. Statistical analysis
392 measured by two-tailed Student's t-test.

393 **Figure 3. N679K results in decreased spike expression on virions and in infected cells.**

394 **(A)** Purified WT, N679K, and Omicron (BA.1) virions from Vero E6 supernatants were probed with
395 α-Spike and α-Nucleocapsid (N) antibodies in Western blots. Full-length spike (FL), S1/S2
396 cleavage product, and S2' cleavage product are indicated.

397 **(B)** Densitometry of spike processing from purified virions applied to Western blots in **(A)** was
398 performed, and quantification of FL and S1/S2 cleavage product percentage of total spike is
399 shown. Quantification was normalized to N as viral protein loading control. WT (black), N679K
400 (green), Omicron (orange). Results are representative of two experiments.

401 **(C)** Densitometry of spike expression from purified virion Western blots in **(A)** was performed, and
402 quantification of total spike protein to nucleocapsid ratio is shown. Spike/N ratio is relative to WT.
403 WT (black), N679K (green), Omicron (orange). Results are representative of two experiments.

404 **(D)** Vero E6 cells were infected with WT, N679K, or Omicron at an MOI of 0.01 infectious
405 units/cell. Cell lysate was collected at 24 hpi and probed with α-Spike and α-Nucleocapsid (N)
406 antibodies in Western blots. Full-length spike (FL), S1/S2 cleavage product, and S2' cleavage
407 product are indicated.

408 **(E)** Densitometry of spike expression from infected cell lysate Western blots in **(D)** was performed,
409 and quantification of total spike protein to nucleocapsid ratio is shown. Spike/N ratio is relative to
410 WT. WT (black), N679K (green), Omicron (orange). Results are representative of three biological
411 replicates.

412 **(F)** Vero E6 cells were infected with WT or N679K at an MOI of 1 infectious units/cell. Cell lysate
413 was collected at 8 hpi in Trizol to extract RNA. RNA transcripts for spike, nucleocapsid and 18S
414 were measured using RT-qpCR. The ratios of ΔΔCt spike to ΔΔCt nucleocapsid are shown. Data
415 are mean ± s.d. Statistical analysis measured by two-tailed Student's t-test.

416 **(G)** Vero E6 cells were transfected with Spike HexaPro WT and N679K and cell lysate was
417 collected at 8, 24, and 48 hpt. Lysates were probed with α-Spike and α-GAPDH antibodies in
418 Western blots.

419 **(H)** Densitometry of spike expression from transfected cell lysates by Western blot in **(G)** was
420 performed, and quantification of relative total spike protein is shown. Spike protein levels were
421 normalized to GAPDH and are relative to WT. WT (black), N679K (green). Results are
422 representative of three biological replicates.

423 **(I)** While WT virus and exogenous spike plasmid produces abundant spike protein, the N679K
424 mutation results in less spike protein expression in virions, intracellularly by infection and
425 transfection of exogenous spike plasmid.

426 **Figure 4. N679K results in preference for upper airways.**

427 **(A)** Schematic of experimental design of transmission competition in golden Syrian hamsters.
428 Donor three- to four-week-old male hamsters were intranasally infected with 10^5 pfu of WT:N679K
429 SARS-CoV-2 in a 1:1 ratio and housed singly. Donors were paired with recipients 24 hpi and
430 cohoused for 8 hrs before separating and nasal washing donors. Nasal washes, tracheas, and
431 lungs were collected at 2 and 4 days post infection for donors (dpi) and post contact for recipients
432 (dpc).

433 **(B)** Next generation sequencing was performed on extracted RNA to measure the percentage of
434 WT (black) and N679K (green) present in nasal wash (left), trachea (middle), and lung (right) of
435 donors (top) and recipients (bottom).

436 **(C)** Immunohistochemistry of left lung lobes at 2, 4 and 7 dpi staining for nucleocapsid. Hamsters
437 were singly infected with 10^5 pfu of either WT or N679K SARS-CoV-2.

438 **(D)** Immunohistochemistry staining of left lung lobes form hamsters infected with WT (black) or
439 N679K (green) SARS-CoV-2 were scored by total section (left), airway (middle), or parenchyma
440 (right) staining. Data are mean showing minimum and maximum (n=5). Statistical analysis
441 measured by two-tailed Student's t-test.

442

443 **Extended Figure 1. Emergence of Omicron subvariants.**

444 **(A)** Timeline of SARS-CoV-2 variants emergence by earliest documented case reported by the
445 WHO.

446 **(B)** Spike mutations across Omicron subvariants with shared mutations across all subvariants
447 (gray box) and mutations unique to the specific variant (bolded) indicated. Mutations key to this
448 study indicated in bold red.

449 **Extended Figure 2. Histopathology of hamsters infected with WT or N679K SARS-CoV-2.**

450 **(A)** H&E staining of left lung of hamsters infected with 10^5 pfu of WT (top) or N679K (bottom)

451 SARS-CoV-2 at 2 (left), 4 (middle), and 7 (right) dpi. Lungs for both WT and N679K show

452 bronchiolitis and interstitial pneumonia at 2 dpi that become more severe at 4 and 7 dpi.

453 **(B)** H&E staining of left lung of hamsters infected with 10^5 pfu of WT (black) or N679K (green)

454 were scored for histopathological analysis.

455

456 **Methods**

457 **Cell Culture**

458 Vero E6 cells were grown in high glucose DMEM (Gibco #11965092) with 10% fetal bovine serum
459 and 1x antibiotic-antimycotic. TMPRSS2-expressing Vero E6 cells were grown in low glucose
460 DMEM (Gibco #11885084) with sodium pyruvate, 10% FBS, and 1 mg/mL Geneticin™ (Invitrogen
461 #10131027). Calu-3 2B4 cells were grown in high glucose DMEM (Gibco #11965092) with 10%
462 defined fetal bovine serum, 1 mM sodium pyruvate, and 1x antibiotic-antimycotic.

463 **Viruses**

464 The SARS-CoV-2 infectious clones were based on the USA-WA1/2020 sequence provided by
465 the World Reference Center of Emerging Viruses and Arboviruses and the USA Centers for
466 Disease Control and Prevention [30]. Mutant viruses (YKH and N679K) were generated with
467 restriction enzyme-based cloning using gBlocks encoding the mutations (Integrated DNA
468 Technologies) and our reverse genetics system as previously described [15,16]. Virus stock was
469 generated in TMPRSS2-exrpressing Vero E6 cells to prevent mutations from occurring at the
470 FCS. Viral RNA was extracted from virus stock and cDNA was generated to verify mutations by
471 Sanger sequencing.

472 Delta isolate (B.1.617.2) was obtained from the World Reference Center of Emerging Viruses and
473 Arboviruses. Infectious clone of Omicron (BA.1) was obtained from Dr. Pei Yong Shi and Dr.
474 Xuping Xie.

475 ***In vitro* Infection**

476 Vira infections in Vero E6 and Calu-3 2B4 were carried out as previously described [8]. Briefly,
477 growth media was removed, and cells were infected with WT or mutant SARS-CoV-2 at an MOI
478 of 0.01 for 45 min at 37°C with 5% CO_2. After absorption, cells were washed three times with PBS
479 and fresh complete growth media was added. Three or more biological replicates were collected
480 at each time point and each experiment was performed at least twice. Samples were titrated with
481 plaque assay or focus forming assays.

482 **Plaque Assay**

483 Vero E6 cells were seeded in 6-well plates and grown to 80-100% confluency in complete growth
484 media. Ten-fold serial dilutions in PBS were performed on virus samples. Growth media was
485 removed from cells and 200 µl of inoculum was added to monolayers. Cells were incubated for
486 45 min at 37°C with 5% CO_2. After absorption, 0.8% agarose overlay was added, and cells were
487 incubated at 37°C with 5% CO_2 for 2 days. Plaques were visualized with neutral red stain. Average
488 plaque size was determined using ImageJ.

489 **Focus Forming Assay**

490 Focus forming assays (FFAs) were performed as previously described [31]. Briefly, Vero E6 cells
491 were seeded in 96-well plates to be 100% confluent. Samples were 10-fold serially diluted in
492 serum-free media and 20 µl was to infect cells. Cells were incubated for 45 min at 37°C with 5%
493 CO_2 before 100 µl of 0.85% methylcellulose overlay was added. Cells were incubated for 24 h 45
494 min at 37°C with 5% CO_2. After incubation, overlay was removed, and cells were washed three
495 times with PBS before fixed and virus inactivated by 10% formalin for 30 min at room temperature.
496 Cells were then permeabilized and blocked with 0.1% saponin/0.1% BSA in PBS before incubated
497 with α-SARS-CoV-2 Nucleocapsid primary antibody (Cell Signaling Technology) at 1:1000 in
498 permeabilization/blocking buffer overnight at 4°C. Cells are then washed three times with PBS
499 before incubated with Alexa Fluor™ 555-conjugated α-mouse secondary antibody (Invitrogen
500 #A28180) at 1:2000 in permeabilization/blocking buffer for 1 h at room temperature. Cells were
501 washed three times with PBS. Fluorescent foci images were captured using a Cytation 7 cell
502 imaging multi-mode reader (BioTek), and foci were counted manually.

503 **Hamster Infection**

504 Three- to four-week-old male golden Syrian hamsters (HsdHan:AURA strain) were purchased
505 from Envigo. All studies were conducted under a protocol approved by the UTMB Institutional
506 Animal Care and Use Committee and complied with USDA guidelines in a laboratory accredited
507 by the Association for Assessment and Accreditation of Laboratory Animal Care. Procedures

508 involving infectious SARS-CoV-2 were performed in the Galveston National Laboratory ABSL3
509 facility. Hamsters were intranasally infected with 10^5 pfu of WT or N679K SARS-CoV-2 in 100 µl.
510 Infected hamsters were weighed and monitored for illness over 7 days. Hamsters were
511 anesthetized with isoflurane and nasal washes were collected with 400 µl of PBS on endpoint
512 days (2, 4, and 7 dpi). Hamsters were euthanized by CO_2 for organ collection. Nasal wash and
513 lung were collected to measure viral titer and RNA. Left lungs were collected for histopathology.

514 **Transmission Competition**

515 Three- to four-week-old male golden Syrian hamsters (HsdHan:AURA strain) were purchased
516 from Envigo. Ten donor hamsters were intranasally infected with a 1:1 ratio of WT:N679K SARS-
517 CoV-2 totaling 10^5 pfu in 100 µl and were subsequently singly housed. After 24 hrs post infection,
518 individual donor hamsters were cohoused with a recipient hamster for 8 hrs for contact
519 transmission. Following 8 hrs, hamster pairs were separated and housed singly, and nasal
520 washes were collected from donors. At 2 and 4 days post infection for donors and post contact
521 for recipients, hamsters were nasal washed with 400 µl of PBS and euthanized for trachea and
522 lung collection. Nasal washes, tracheas, and lungs were processed in TRIzol and RNA was
523 extracted to perform next generation sequencing.

524 **Virion Purification**

525 Vero E6 cells were grown in T175 flasks to be 100% confluent at time of infection. Cells were
526 infected with 50 µl of virus stock in PBS for 45 min at 37°C with 5% CO_2, and growth media with
527 5% FBS was added after absorption. Supernatant was harvested at 24 hpi and clarified by low-
528 speed centrifugation. Virions were purified from supernatant by ultracentrifugation through a 20%
529 sucrose cushion at 26,000 rpm for 3 hrs using a Beckman SW28 rotor. Pellets were resuspended
530 with 2x Laemmli buffer to obtain protein samples for Western blot.

531 **Western Blot**

532 Protein levels were determined by SDS–PAGE followed by western blot analysis as previously
533 described [8]. In brief, sucrose-purified SARS-CoV-2 virions were inactivated by resuspending in

534 2x Laemmli buffer and boiling. SDS-PAGE gels were run with equal volumes of samples on Mini-
535 PROTEAN TGX gels (Bio-Rad #4561094) followed by transfer onto PVDF membrane.
536 Membranes were incubated with α-SARS-CoV S primary antibody (Novus Biologicals #NB100-
537 56578) at 1:1000 dilution in 5% BSA in TBST to measure spike protein processing and
538 expression. For loading control, α-SARS Nucleocapsid primary antibody (Novus Biologicals
539 #NB100-56576) at 1:1000 in 5% BSA in TBST was used for viral loading control and α-GAPDH
540 primary antibody (Invitrogen #AM4300) at 1:1000 in 5% BSA in TBST for cellular loading control.
541 Primary antibody incubation was followed by HRP-conjugated α-rabbit secondary antibody (Cell
542 Signaling Technology #7074) or HRP-conjugated α-mouse secondary antibody (Cell Signaling
543 Technology #7076) at 1:3000 in 5% milk in TBST. Chemiluminescence signal was developed
544 using Clarity Western ECL substrate (Bio-Rad #1705060) or Clarity Max Western ECL substrate
545 (Bio-Rad #1705062) and imaged with a ChemiDoc MP System (Bio-Rad). Densitometry analysis
546 was performed using ImageLab 6.0.1 (Bio-Rad).

547 **RT-qPCR**

548 Vero E6 cells were infected with an MOI of 1 as detailed above in *in vitro* infection. Cell lysate
549 was collected at 8 hpi in TRIzol. RNA was extracted from TRIzol samples using Direct-zol RNA
550 Miniprep Plus kit (Zymo #R2072) to be used in two-step RT-qPCR. cDNA was reverse transcribed
551 from 1 µg of total RNA using LunaScript RT Supermix kit (NEB #E3010) according to
552 manufacturer's instructions. RT-qPCR was performed using Luna Universal qPCR Master mix
553 (NEB #M3003) according to manufacturer's instructions. RT-qPCR cycle was performed as
554 follows: 95°C for 60 s (1 cycle), 95°C for 15 s and 51°C for 30 s then plate read (40 cycles), and
555 melt curve from 65°C to 95°C for 5 s. For spike and nucleocapsid transcripts, a forward primer
556 binding upstream of the transcription regulatory sequence (TRS) leader region
557 (ACCAACCAACTTTCGATCTCT) was used with reverse primers for spike
558 (TGCAGGGGGTAATTGAGTTCT) and nucleocapsid (CCCACTGCGTTCTCCATTCT). The 18S
559 ribosomal RNA primers were forward (CCGGTACAGTGAAACTGCGAATG) and reverse

560 ((GTTATCCAAGTAGGAGAGGAGCGAG). RNA transcript levels for spike and nucleocapsid
561 were determined by ΔΔCt method with 18S as the internal control. Ratios of ΔΔCt spike over
562 ΔΔCt nucleocapsid was reported for each sample.

563 **Spike HexaPro Cloning and Transfection**

564 SARS-CoV-2 S HexaPro was a gift from Jason McLellan (Addgene plasmid #154754) [21]. The
565 N679K mutation was cloned into spike HexaPro using a gBlock encoding the mutation (Integrated
566 DNA Technologies) and restriction enzyme-based cloning. Sequences were verified by Sanger
567 sequencing.

568 Vero E6 cells were grown in 24-well plates to be 100% confluent at time of transfection. Cells
569 were transfected with spike HexaPro WT or N679K plasmid and Lipofectamine 2000 following
570 manufacturer's instructions (Invitrogen). Briefly, 100 ng of spike HexaPro plasmid and 1.5 µl of
571 Lipofectamine 2000 were separately diluted in 50 µl Opti-MEM (Gibco #31985070) before mixing
572 together. After 20 min of room temperature incubation, 100 µl of the transfection mixture was
573 added to cells, and cells were incubated at 37°C with 5% CO_2. Cell lysate was harvested with 2x
574 Laemmli buffer at 24 and 48 hours post transfection to be analyzed by Western blot.

575 **Structural Modeling**

576 Structural models previously generated were used as a base to visualize residues mutated in
577 Omicron [8]. Briefly, structural models were generated using SWISS-Model to generate homology
578 models for WT and glycosylated SARS-CoV-2 spike protein on the basis of the SARS-CoV-1
579 trimer structure (Protein Data Bank code 6ACD). Homology models were visualized and
580 manipulated in PyMOL (version 2.5.4) to visualize Omicron mutations.

581 **Next Generation Sequencing**

582 Next generation sequencing to determine viral RNA populations was performed as previously
583 described [31]. Briefly, RNA samples were extracted and prepared for Tiled-ClickSeq libraries [32]. A
584 modified pre-RT annealing protocol was applied as previously described[31]. The final libraries
585 comprising of 300–700 bps fragments were pooled and sequenced on an Illumina NextSeq

586 platform with paired-end sequencing. The raw Illumina data of the Tiled-ClickSeq libraries were
587 processed with previously established bioinformatics pipelines[32]. One modification is the
588 introduction of ten wild cards ("N") covering the N679K mutation in the reference genome to allow
589 *bowtie2*[33] to align reads to wild type or variant genomes without bias. PCR duplications were
590 removed using *UMI-tools*[34], and the number of unique reads representing WT and N679K variants
591 were counted thereafter.

592 **Histology**

593 Left lung lobes were harvested from hamsters and fixed in 10% buffered formalin solution for at
594 least 7 days. Fixed tissue was then embedded in paraffin, cut into 5 μM sections, and stained with
595 hematoxylin and eosin (H&E) on a SAKURA VIP6 processor by the University of Texas Medical
596 Branch Surgical Pathology Laboratory.

597 **Immunohistochemistry**

598 Fixed and paraffin-embedded left lung lobes from hamsters were cut into 5 μM sections and
599 mounted onto slides by the University of Texas Medical Branch Surgical Pathology Laboratory.
600 Paraffin-embedded sections were warmed at 56°C for 10 min, deparaffinized with xylene (3x 5-
601 min washes) and graded ethanol (3x 100% 5-min washes, 1x 95% 5-min wash), and rehydrated
602 in distilled water. After rehydration, antigen retrieval was performed by steaming slides in antigen
603 retrieval solution (10 mM sodium citrate, 0.05% Tween-20, pH 6) for 40 min (boil antigen retrieval
604 solution in microwave, add slides to boiling solution, and incubate in steamer). After cooling and
605 rinsing in distilled water, endogenous peroxidases were quenched by incubating slides in TBS
606 with 0.3% H_2O_2 for 15 min followed by 2x 5-min washes in 0.05% TBST. Sections were blocked
607 with 10% normal goat serum in BSA diluent (1% BSA in 0.05% TBST) for 30 min at room
608 temperature. Sections were incubated with primary anti-N antibody (Sino #40143-R001) at 1:1000
609 in BSA diluent overnight at 4°C. Following overnight primary antibody incubation, sections were
610 washed 3x for 5 min in TBST. Sections were incubated in secondary HRP-conjugated anti-rabbit
611 antibody (Cell Signaling Technology #7074) at 1:200 in BSA diluent for 1 hour at room

612 temperature. Following secondary antibody incubation, sections were washed 3x for 5 min in
613 TBST. To visualize antigen, sections were incubated in ImmPACT NovaRED (Vector Laboratories
614 #SK-4805) for 3 min at room temperature before rinsed with TBST to stop the reaction followed
615 by 1x 5-min wash in distilled water. Sections were incubated in hematoxylin for 5 min at room
616 temperature to counterstain before rinsing in water to stop the reaction. Sections were dehydrated
617 by incubating in the previous xylene and graded ethanol baths in reverse order before mounted
618 with coverslips.

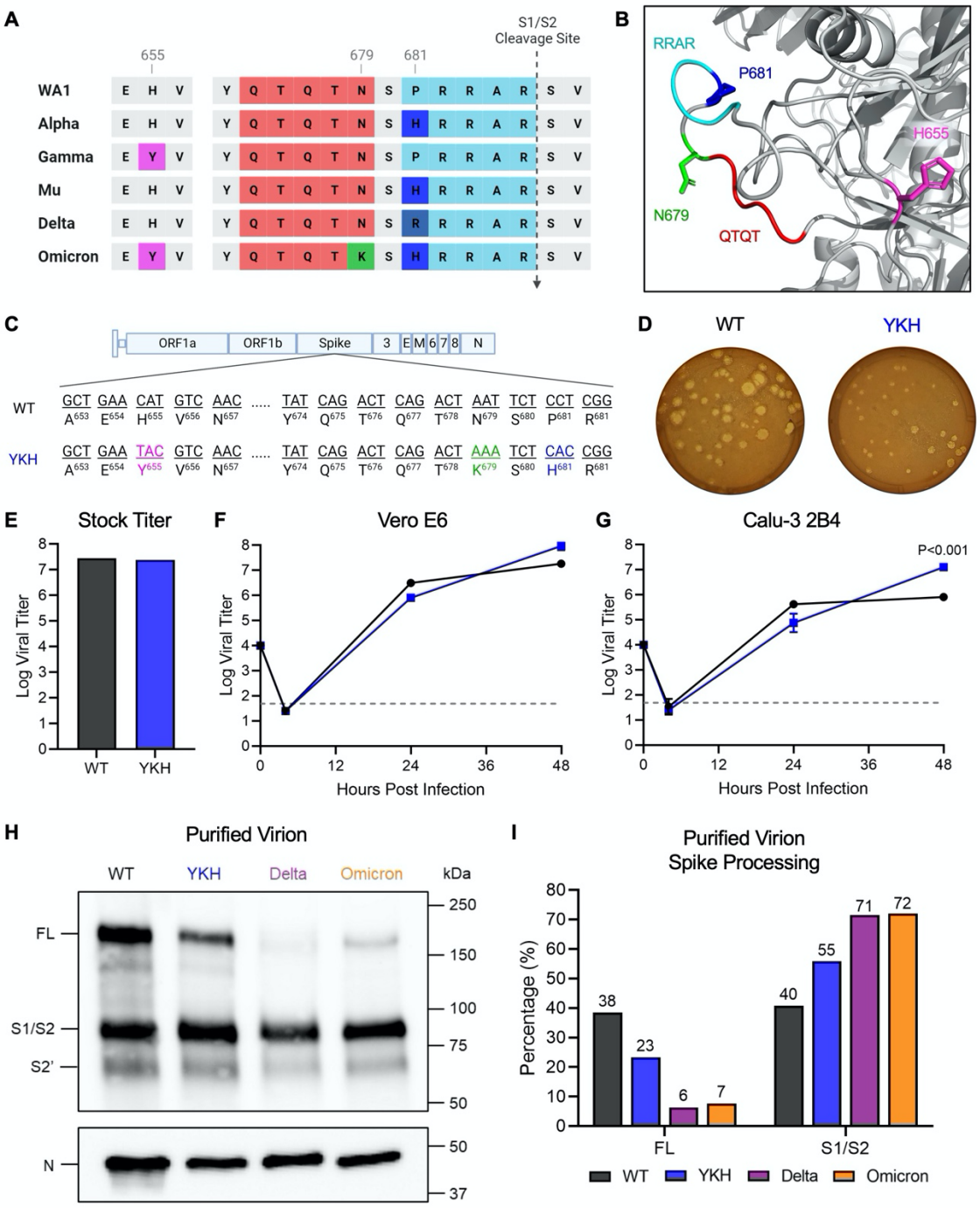

Figure 1. The combination of Omicron mutations H655Y, N679K, and P681H increases viral replication and spike processing. **(A)** Comparison of CTS1 region near the S1/S2 cleavage site between SARS-CoV-2 variants. **(B)** Structure of loop containing the S1/S2 cleavage site on SARS-CoV-2 spike protein. The residues that are mutated in Omicron are shown – H655 (magenta), N679 (green), and P681 (blue). The furin cleavage site RRAR (cyan) and QTQT motif (red) are also shown. **(C)** Schematic of WT and YKH SARS-CoV-2 mutant genomes. **(D)** WT and YKH SARS-CoV-2 plaques on Vero E6 cells at 2 dpi. **(E)** Viral titer from WT and YKH virus stock with the highest yield generated from TMPRSS2-expressing Vero E6 cells. **(F-G)** Growth kinetics of WT and YKH in Vero E6 **(F)** and Calu-3 2B4 **(G)** cells. Cells were infected at an MOI of 0.01 (n=3). Data are mean ± s.d. Statistical analysis measured by two-tailed Student's t-test. **(H)** Purified WT, YKH, Delta isolate (B.1.617.2), and Omicron (BA.1) virions from Vero E6 supernatant were probed with α-Spike and α-Nucleocapsid (N) antibodies in Western blots. Full-length spike (FL), S1/S2 cleavage product, and S2' cleavage product are indicated. **(I)** Densitometry of FL and S1/S2 cleavage product was performed, and quantification of FL and S1/S2 cleavage product percentage of total spike is shown. Quantification was normalized to N for viral protein loading control. WT (black), YKH (blue), Delta isolate (purple), Omicron (orange). Results are representative of two experiments.

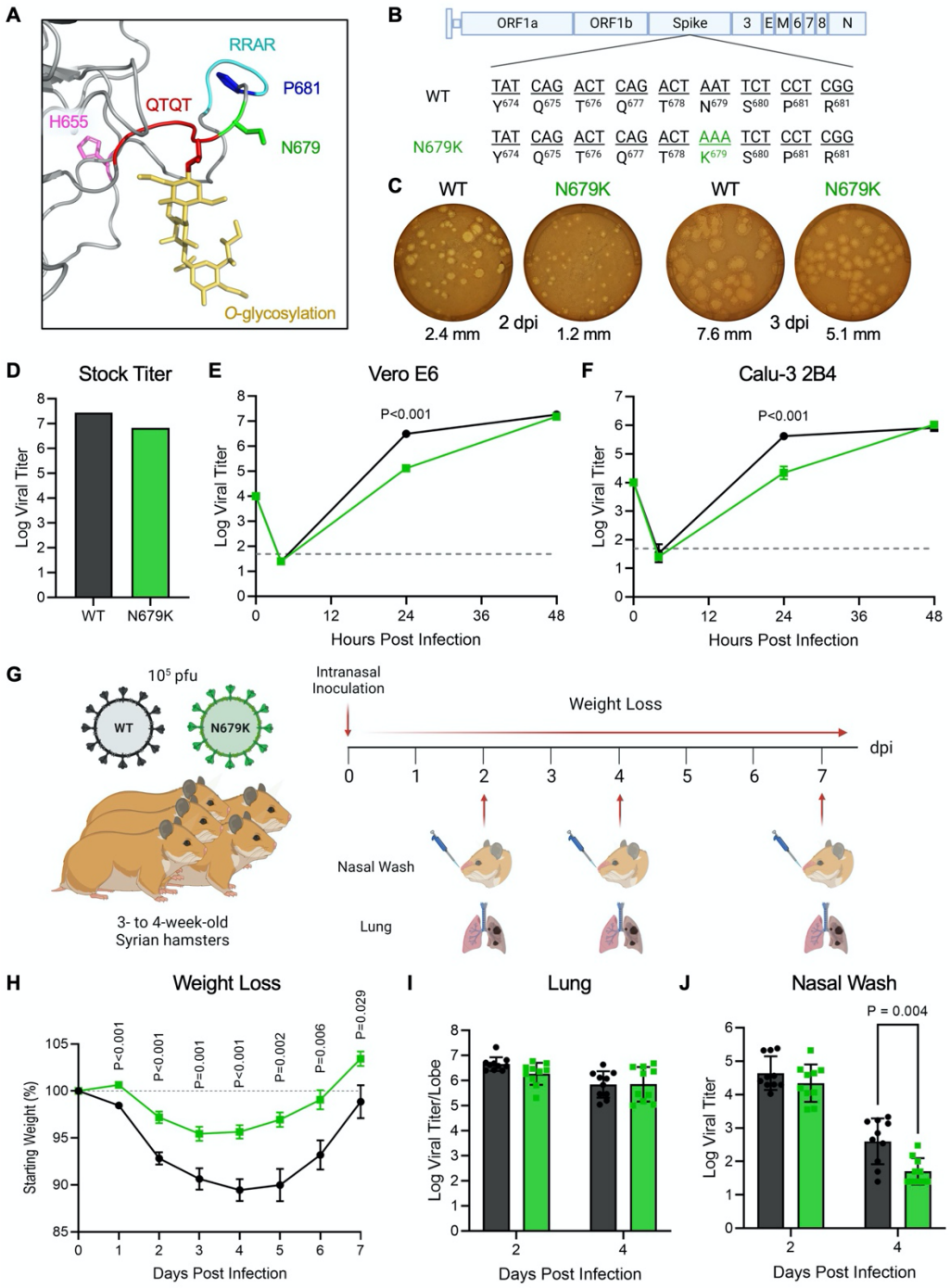

Figure 2. N679K attenuates SARS-CoV-2 replication and disease when isolated.
(A) Structural modeling of O-linked glycosylation of threonine 678 (yellow) of QTQTN motif (red) and the residues mutated in Omicron – H655 (magenta), N679 (green), and P681 (blue) – with N679 adjacent to the glycosylation. The furin cleavage site RRAR is also shown (cyan). **(B)** Schematic of WT and N679K SARS-CoV-2 genomes. **(C)** WT and N679K SARS-CoV-2 plaques on Vero E6 cells at 2 dpi (left) and 3 dpi (right). Average plaque size noted below. **(D)** Viral titer from WT and N679K virus stock with the highest yield generated form TMPRSS2-expressing Vero E6 cells. **(E-F)** Growth kinetics of WT and N679K in Vero E6 **(E)** and Calu-3 2B4 **(F)** cells. Cells were infected at an MOI of 0.01 (n=3). Data are mean ± s.d. Statistical analysis measured by two-tailed Student's t-test. **(G)** Schematic of experiment design for golden Syrian hamster infection with WT (black) or N679K (green) SARS-CoV-2. Three- to four-week-old make hamsters were infected with 10^5 pfu and monitored for weight loss over 7 days. At 2, 4, and 7 dpi, nasal wash and lung was collected for viral titer, and lung was collected for histopathology. **(H)** Weight loss of hamsters infected with WT (black) or N679K (green) SARS-CoV-2 over 7 days. Data are mean ± s.e.m. Statistical analysis measured by two-tailed Student's t-test. **(I-J)** Viral titer of lung **(I)** and nasal wash **(J)** collected at 2 and 4 dpi from hamsters infected with WT (black) or N679K (green) SARS-CoV-2. Data are mean ± s.d. Statistical analysis measured by two-tailed Student's t-test.

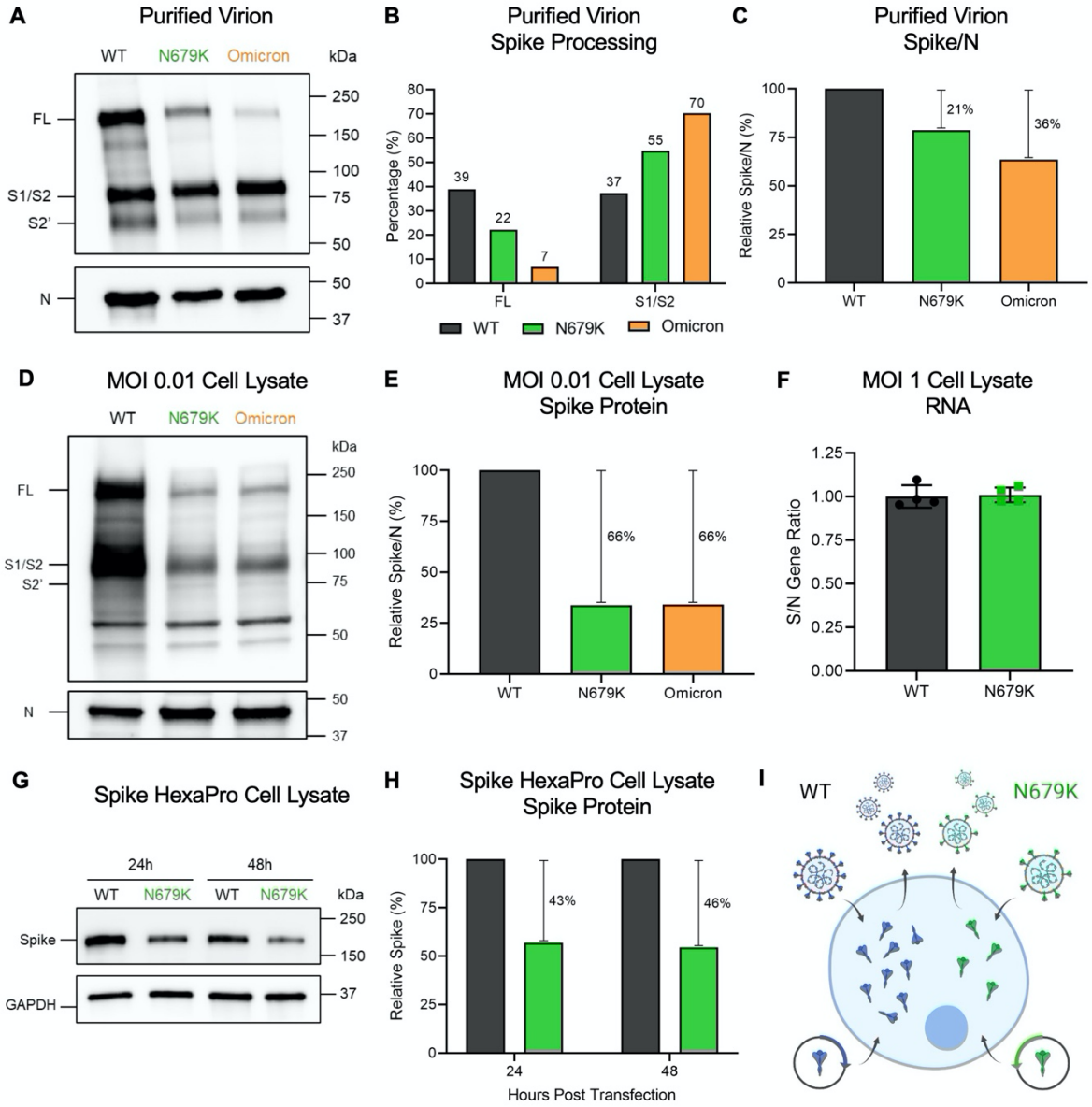

Figure 3. N679K results in decreased spike expression on virions and in cell lysate.
(A) Purified WT, N679K, and Omicron (BA.1) virions from Vero E6 supernatant were probed with α-Spike and α-Nucleocapsid (N) antibodies in Western blots. Full-length spike (FL), S1/S2 cleavage product, and S2' cleavage product are indicated. **(B)** Densitometry of spike processing from purified virion Western blot in **(A)** was performed, and quantification of FL and S1/S2 cleavage product percentage of total spike is shown. Quantification was normalized to N as viral protein loading control. WT (black), N679K (green), Omicron (orange). Results are representative of two experiments. **(C)** Densitometry of spike expression from purified virion Western blot in **(A)** was performed, and quantification of total spike protein to nucleocapsid ratio is shown. Spike/N ratio is relative to WT. WT (black), N679K (green), Omicron (orange). Results are representative of two experiments. **(D)** Vero E6 cells were infected with WT, N679K, or Omicron at an MOI of 0.01. Cell lysate was collected at 24 hpi and probed with α-Spike and α-Nucleocapsid (N) antibodies in Western blots. Full-length spike (FL), S1/S2 cleavage product, and S2' cleavage product are indicated. **(E)** Densitometry of spike expression from infected cell lysate Western blot in **(D)** was performed, and quantification of total spike protein to nucleocapsid ratio is shown. Spike/N ratio is relative to WT. WT (black), N679K (green), Omicron (orange). Results are representative of three biological replicates. **(F)** Vero E6 cells were infected with WT or N679K at an MOI of 1 infectious units/cell. Cell lysate was collected at 8 hpi in Trizol to extract RNA. RNA transcripts for spike, nucleocapsid and 18S were measured using RT-qpCR. The ratios of ΔΔCt spike to ΔΔCt nucleocapsid are shown. Data are mean ± s.d. Statistical analysis measured by two-tailed Student's t-test. **(G)** Vero E6 cells were transfected with Spike HexaPro WT and N679K and cell lysate was collected at 8, 24, and 48 hpt. Lysates were probed with α-Spike and α-GAPDH antibodies in Western blots. **(H)** Densitometry of spike expression from transfected cell lysates by Western blot in **(G)** was performed, and quantification of relative total spike protein is shown. Spike protein levels were normalized to GAPDH and are relative to WT. WT (black), N679K (green). Results are representative of three biological replicates. **(I)** While WT virus and exogenous spike plasmid produces abundant spike protein, the N679K mutation results in less spike protein expression in virions and intracellularly by infection and transfection of exogenous spike plasmid.

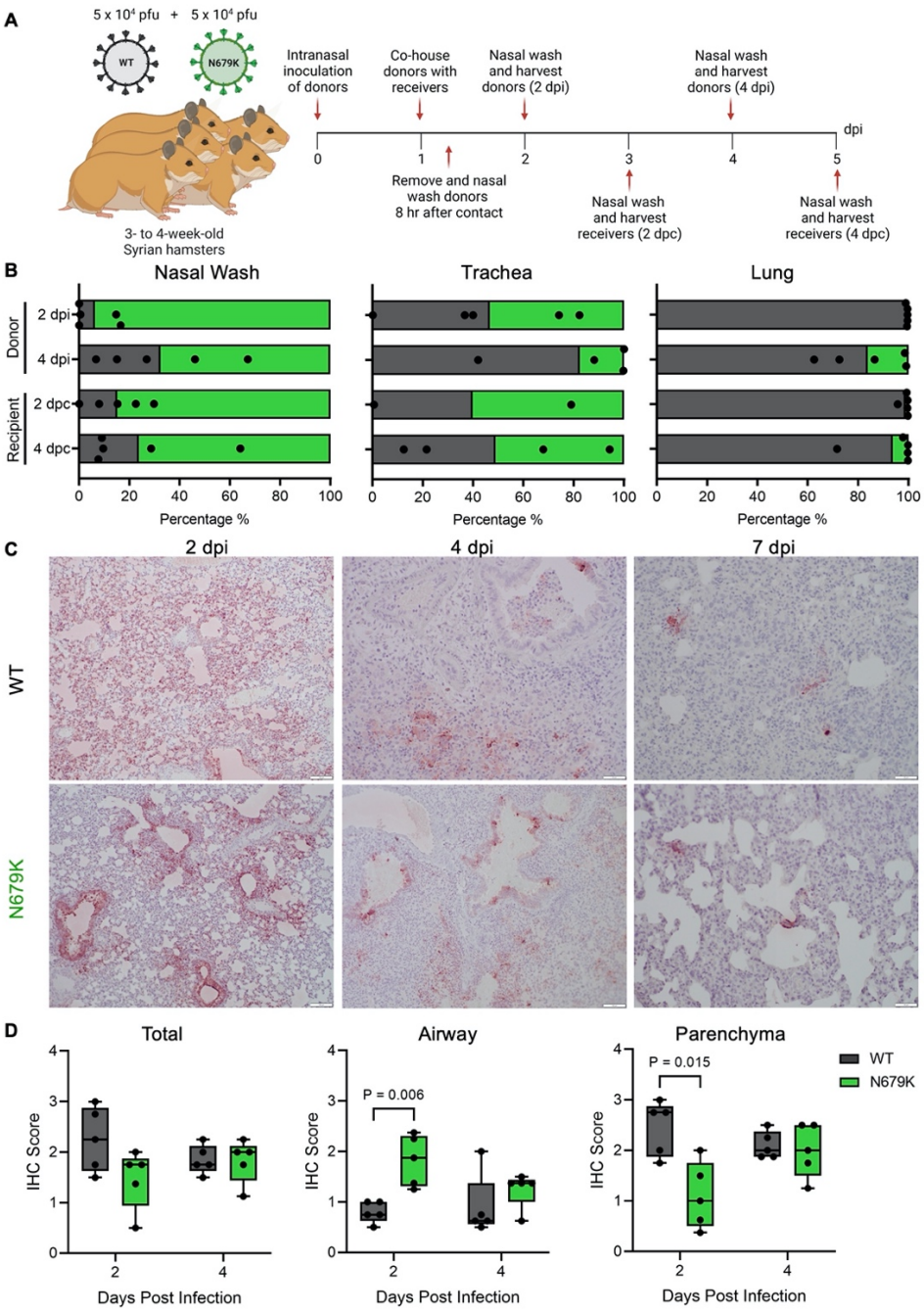

Figure 4. N679K results in preference for upper airways.
(A) Schematic of experimental design of transmission competition in golden Syrian hamsters. Donor three- to four-week-old male hamsters were intranasally infected with 10^5 pfu of WT:N679K SARS-CoV-2 in a 1:1 ratio and housed singly. Donors were paired with recipients 24 hpi and cohoused for 8 hrs before separating and nasal washing donors. Nasal washes, tracheas, and lungs were collected at 2 and 4 days post infection for donors (dpi) and post contact for recipients (dpc).
(B) Next generation sequencing was performed on extracted RNA to measure the percentage of WT (black) and N679K (green) present in nasal wash (left), trachea (middle), and lung (right) of donors (top) and recipients (bottom).
(C) Immunohistochemistry of left lung lobes at 2, 4 and 7 dpi staining for nucleocapsid. Hamsters were singly infected with 105 pfu of either WT or N679K SARS-CoV-2.
(D) Immunohistochemistry staining of left lung lobes form hamsters infected with WT (black) or N679K (green) SARS-CoV-2 were scored by total section (left), airway (middle), or parenchyma (left) staining. Data are mean showing minimum and maximum (n=5). Statistical analysis measured by two-tailed Student's t-test.

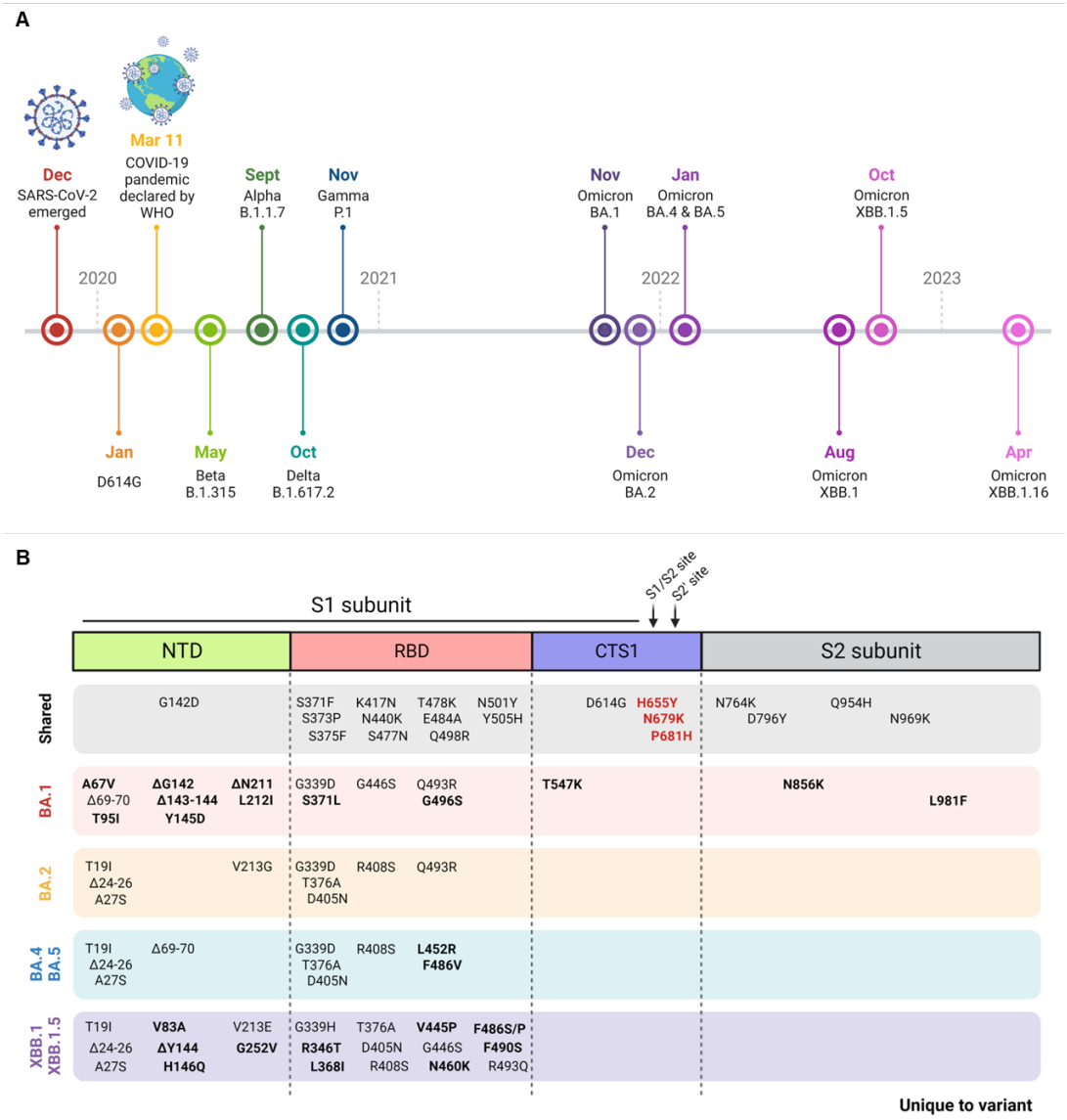

Extended Figure 1. Emergence of Omicron subvariants.
(A) Timeline of SARS-CoV-2 variants emergence by earliest documented case reported by the WHO.
(B) Spike mutations across Omicron subvariants with shared mutations across all subvariants (gray box) and mutations unique to the specific variant (bolded) indicated. Mutations key to this study indicated in bold red.

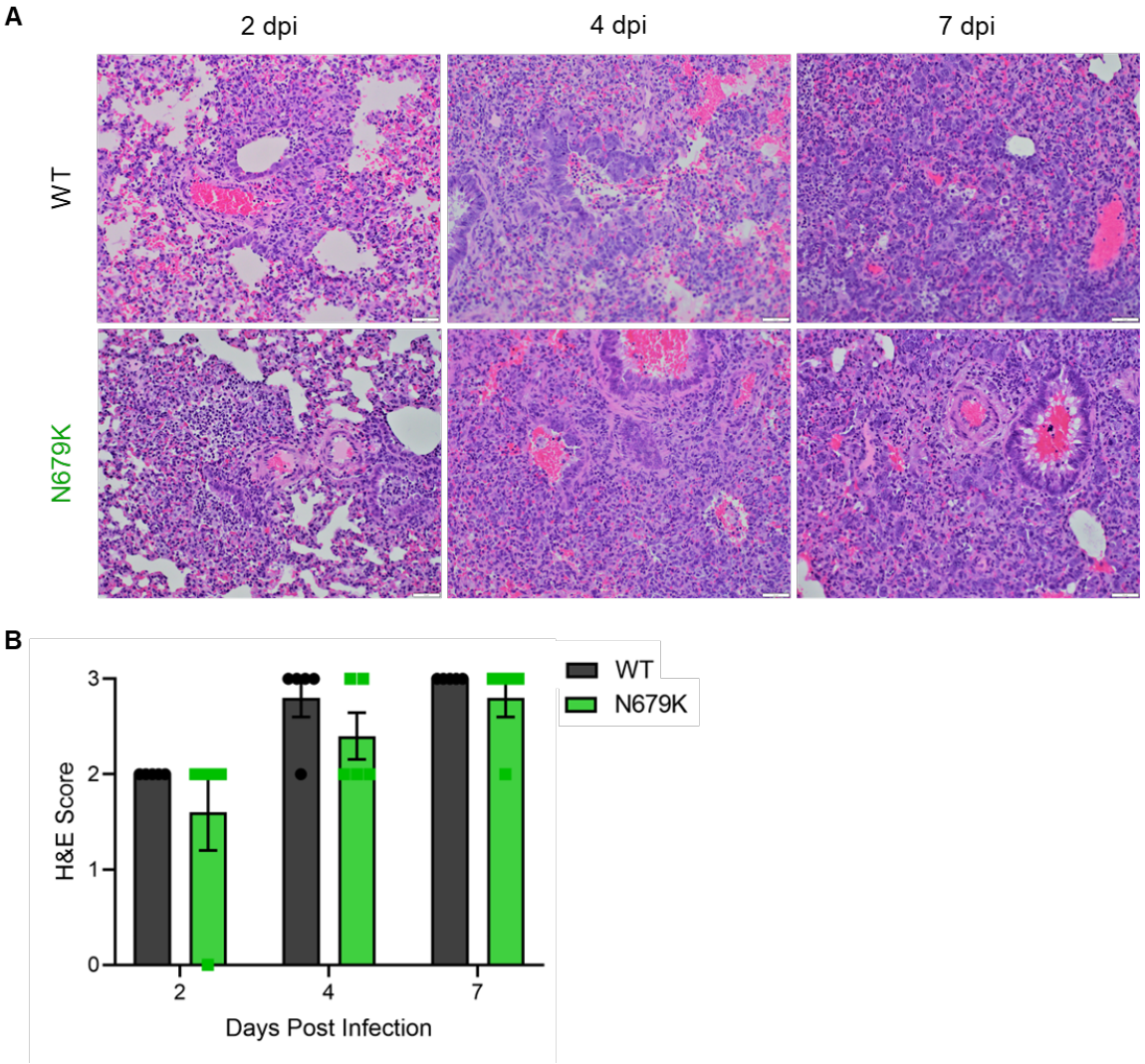

Extended Figure 2. Histopathology of hamsters infected with WT or N679K SARS-CoV-2.
(A) H&E staining of left lung of hamsters infected with 10^5 pfu of WT (top) or N679K (bottom) SARS-CoV-2 at 2 (left), 4 (middle), and 7 (right) dpi. Lungs for both WT and N679K show bronchiolitis and interstitial pneumonia at 2 dpi that become more severe at 4 and 7 dpi.
(B) H&E staining of left lung of hamsters infected with 10^5 pfu of WT (black) or N679K (green) were scored for histopathological analysis.